ORIGINAL ARTICLE

Determination of the optimum filter for ^{99m}Tc SPECT breast imaging using a wire mesh collimator

Xianling Dong[1,2]*, M.I. Saripan[3], R. Mahmud[4], S. Mashohor[3], Aihui Wang[5]

[1]Insititute of Advanced Technology, Universiti Putra Malaysia, Serdang, Malaysia. [2]Department of Biomedical Engineering, Chengde Medical University, China. [3]Faculty of Engineering, Universiti Putra Malaysia, Serdang, Malaysia. [4]Faculty of Medicine and Sciences, Universiti Putra Malaysia, Serdang, Malaysia. [5]Department of Nuclear Medicine, Affiliated Hospital, Chengde Medical University, China.

ABSTRACT

Background: The development of wire mesh collimator (WMC), has improved the performance of Single Photon Emission Computed tomography (SPECT) because of its higher sensitivity whilst maintaining the same resolution. Consequently, the WMC allows better detection of early–stage cancer. The purpose of this study was to find an optimal filter for image reconstruction for breast SPECT imaging.

Methods: Half–ellipsoidal breast phantom in the prone position was simulated with dual–head SPECT camera by Monte Carlo N–Particle Transport Code, version 5 (MCNP5). Six different filters were compared with 17 different cutoff frequencies (Fc), ranging from 0.2 Nyquist frequency (Nq) to 1.0 Nq, with step 0.05. For Butterworth filter, order was from 3 to 12 with step 1. A total of 255 central slices with different parameters were reconstructed by filtered back projection (FBP) to compare the image performance in terms of contrast, noise level and tumour size.

Results: The values of tumour size, contrast and noise level were greatly influenced by different filter types and the value of Fc. Ramp and Butterworth produced the best value of tumour size and contrast, whilst Parzen, Hann and Hamming filters gave smoother images. Overall, results showed that Butterworth filter with the highest mean score.

Conclusion: Butterworth filter proved to be the provided the best image quality at a higher sensitivity and was found to be the optimum filter for quantitative analysis.

Keywords: Wire mesh collimator, SPECT breast imaging, filtering, Cut–off frequency

INTRODUCTION

In breast SPECT imaging, projections are obtained from many angles around the breast, and then these data are reconstructed to form the tomographic images by reconstruction techniques such as filtered back projection or iterative methods. Imaging filtering is a key element of image reconstruction process and is intimately related to optimum image quality. A well–known filter, named as Ramp filter, is a type of a high–pass filter that reduce the 1/r blurring effect and preserves high frequencies, while filters like Parzen, Hann, Hamming, Shepp–logan, and Butterworth are all low–pass filters, which act as a function window that can preserve low–frequency structures and diminishing high–frequency noise [1,2]. Typical filters commonly used in commercial software package are the product of ramp and one of the five low–pass filters, as shown in Figure 1.

WMC is a newly designed collimator to replace the conventional low–energy high–resolution (LEHR) parallel–hole collimators on gamma cameras. Previously, this collimator had only been tested for 2D planar imaging of breast cancers [3–6]. There are multiple reports of SPECT imaging of breast cancers in the literature [7–10]. However, none of the studies have investigated the characteristics of the filter techniques during image reconstruction process. The choice of filter is usually a compromise between the noise and fine detail suppression of the image area of interest. In clinical practice, several factors would affect the choice of filter [1,11], such as the number of counts, the background noise level, the organs being imaged, the energy of the isotopes, and the type of collimator. In this study, we intended to find the optimum filter for SPECT breast imaging with WMC using technetium–99m source in Monte Carlo simulation environment.

MATERIALS AND METHODS

Monte Carlo simulation

The SIEMENS Symbia T camera is a dual–head SPECT camera, which consists of a removable LEHR collimator, a sodium iodide (NaI) scintillation crystal, a light guide and an array of PMT [12]. The detector is filled with NaI with density of 3.67g/cm^3 and size 0.9525 cm in thickness, 53.3x38.7 cm^2 in area. Based on this camera, MCNP5 [13]

Address for correspondence
Dong Xianling
Insititute of Advanced Technology
Universiti Putra Malaysia
43300 Sri Serdang,
Selangor, Malaysia
Email: dongxl_cdmc@163.com

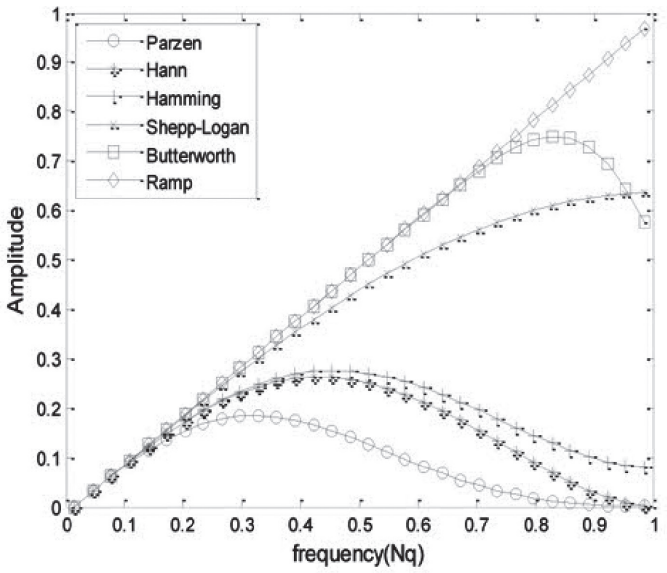

Figure 1. Six commonly used filters in SPECT image reconstruction

was used to simulate the geometry structure of SPECT camera with a WMC. The WMC is a parallel and square hole type of collimator, which has 101 interchangeable layers of wire with the hole size 0.15 cm, septa size 0.02 cm and a thickness of 4cm [6]. The geometry of SPECT camera and side view of WMC is shown in Figure 2(a). The pixel size is 0.48 cm, and a hardware zoom factor of 1.23 was applied, thus yielding a pixel size with 0.39 cm [14,15]. A Pyrex slab with a density of 1.4718 g/cm^3 and thickness of 6.6 cm was used to address the issue of backscatter by modelling the backscattering effect due to the light pipe, PMTs, mu–metal magnetic shielding or other structures in a real camera [16].

Half–ellipsoidal breast phantom, a close approximation of the real breast was used to simulate the clinical examination for breast cancer in the prone position [5]. Based on the early stage of TNM system [17,18], a stage 1 tumour was investigated in this study and a spherical tumour located in the center of breast phantom with diameter 1.5 cm was simulated.

In order to make the simulation approximately close to the real situation, the activity of breast should be assigned properly. For breast imaging, in general a 20 mCi (740 MBq) dose of technetium–99m is injected and the patient rests for several minutes to allow thorough distribution of the radiotracer [19–22]. To approximate the activity concentration expected from volumetric breast SPECT, the activity in the breast is converted to units of µCi/mL. Many efforts had been done to measure the activities in the breast [19,22,23], and the activity was about 80 nCi/mL for breast normal tissue. This activity had also been used in other studies [3,5,24].

Data collection

Every projection set was acquired with 120 angles over 360 degrees with an angle step of 3o for each projection. The method to generate the projections from the MCNP5 simulation output files followed the previous study [25].

After collecting all the projections, filter was applied to the original projections. Finally, inverse radon transformation was performed to generate the cross–sectional images of the breast phantom. Figure 3 shows the overall flow chart of methodology in this study.

The transaxial slices were obtained by image reconstruction using filtered back projection with matrix of 64x64, which yields a voxel size of 0.39x0.39x0.39 cm^3. Images were corrected by attenuation correction based on Chang's method [26] with a linear attenuation coefficient of 0.12^{-1} cm [2,11,27]. No scatter correction was applied in this study.

Filter evaluation

Six different filters were compared with 17 different Fc, ranging from 0.2 Nq to 1.0 Nq, with step 0.05. For Butterworth filter, order was from 3 to 12 with step 1. A total of 255 central slices with different filter parameters were reconstructed to compare the performance in terms of contrast, noise level and tumour size.

Tumour size was determined using full width at half maximum (FWHM) of the four directions of profiles (0°, 45°, 90° and 135°) in the central slice image, purple dotted lines as shown in Figure 5. Carrie *et al.* [28] stated the correlation between the measured full width at 25%, 35%, and 50% of the maximum intensity

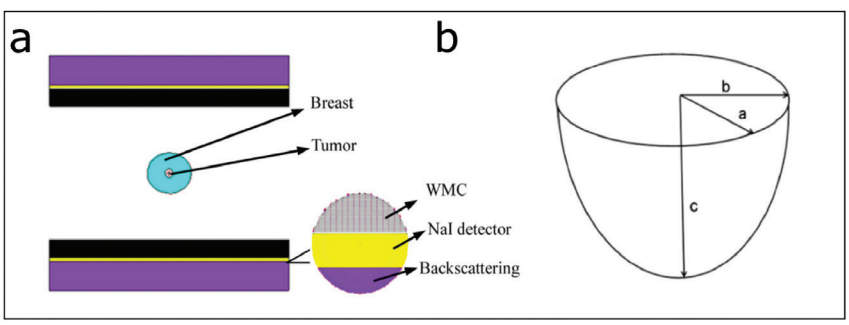

Figure 2. (a) Geometry of dual–head SPECT camera with WMC as viewed by VisEd; (b) Half–ellipsoidal geometry for breast phantom

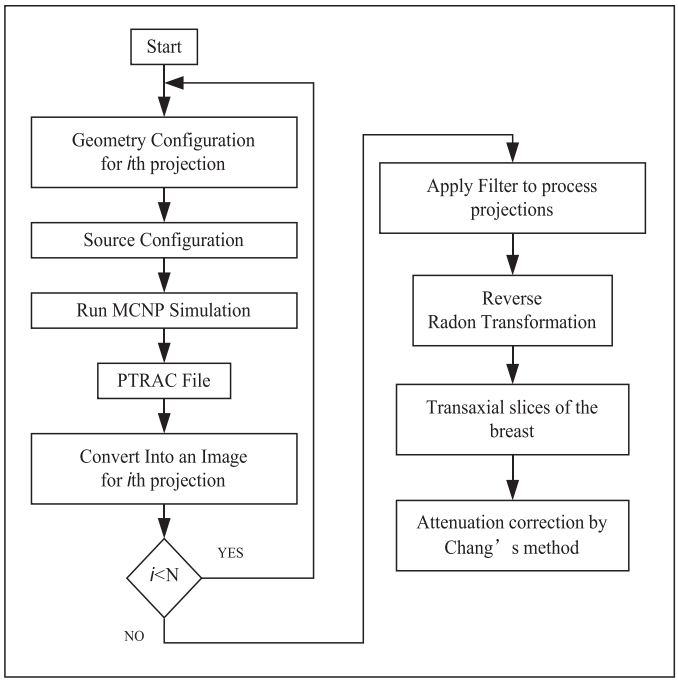

Figure 3. Flow chart of image reconstruction in the simulation

profiles at various breast thicknesses and true tumour diameter. Based on that, full width at 35% of the maximum was used to determine the true tumour size. The terms, contrast and noise level were calculated in the following equations:

$$C = \frac{R_o - R_b}{R_b} \quad (1)$$

where, R_o is the mean value in the tumour area (regions shown by yellow arrow), while R_b is the mean value in the normal breast tissue (four green rectangular regions shown in Figure 4).

$$N = \frac{\sigma_b}{R_b} \quad (2)$$

where σ_b is the standard deviation of the normal breast tissue. This term also refers to coefficient of variation.

The determination of the optimum filter for SPECT breast imaging would consider the ability of each filter type in producing high contrast, low noise, and approximate tumour size. Therefore, the total grade (trade off between contrast, noise level, and tumour size) was analyzed. To calculate the total grade, the grading method used by Takavar et al. [29] was applied. For every filter, each parameter was first graded from 1 to 100 contrast and noise (1 for worst and 100 for the best) , while 1 for the biggest and 100 for the nearest tumour size to the true size.

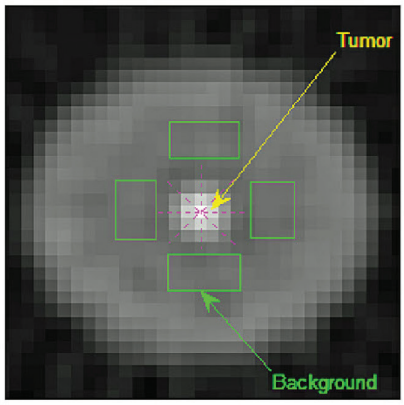

Figure 4. Regions of tumour and background in the central slice

RESULTS

Tumour size

One example of determined tumour size by different Fc of Butterworth filter with order 6 was shown in Figure 5. Low Fc smoothed the slice in a high degree so that it led to extended tumour size. As the Fc increased, spatial resolution was improved and acceptable tumour size was obtained from Fc range of 0.55Nq to 0.8 Nq, which yielded a tumour size about 1.6 cm. Due to high level noise, the tumour size started to increase when Fc was higher than 0.8 Nq.

As can be seen from Table 1, the nearest FWHM to real tumour size was obtained by Ramp and Butterworth

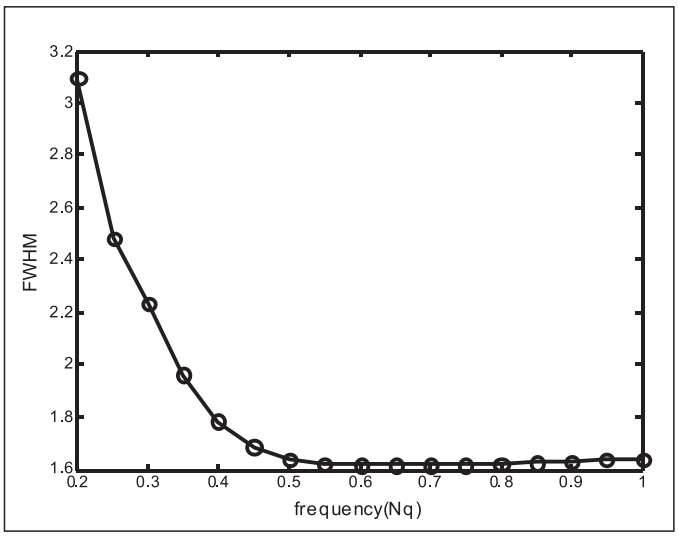

Figure 5. FWHM obtained at different Fc of Butterworth filter

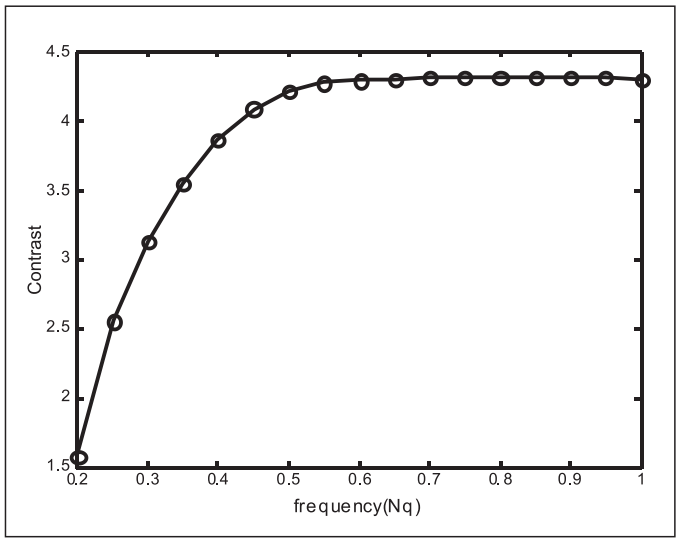

Figure 6. Contrast obtained at different Fc of Butterworth filter

filters, which was about 1.6 cm, followed by Shepp–Logan filter. The rest of the filters did not provide an approximation between the tumour size on imaging with the actual tumour size. The lower Fc we set, the bigger the tumour size obtained. Thus, the difference between maximum and minimum value of tumour size was due to value of Fc. When a very small Fc was selected, the tumour size was almost double the real size or even bigger, which did not correspond with the clinically known tumour size. In addition, Butterworth filter yielded lowest standard derivation (SD) of 0.39, which indicated the value of Fc has less effect on tumour size than the other five filters.

Contrast

Smoothing in a high degree by low Fc lost mage contrast, as shown in Figure 6. the contrast was only 1.5 when Fc was 0.2 Nq. As Fc increased, slices with high contrast were obtained. Contrast was saturated at maximum value about 4.3 when Fc was bigger than 0.55 Nq.

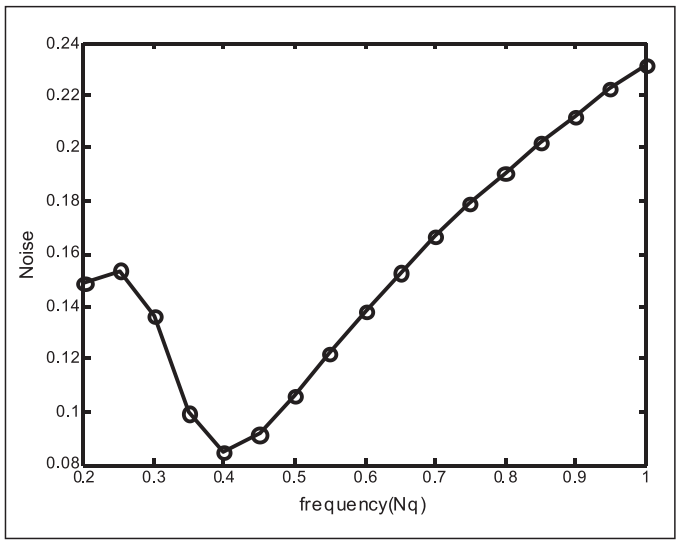

Figure 7. Noise level obtained at different Fc of Butterworth filter

Table 2 summarizes the contrast for six filters. Ramp filter and Butterworth almost got the highest contrast, followed by Shepp–Logan filter. The rest of the three filters, yielded a lower contrast. When a low Fc was selected, slice image was dramatically smoothed. As we can see, the minimum value of contrast for Parzen, Hann and Hamming filters was about 0.6, which was substantially decreased the tumour visibility. Again, Butterworth obtained the lowest value of SD.

Noise

Low Fc generally eliminated noise effectively and led to a smoothing of the image. However, as we can see from Figure 7, the minimum noise level was obtained at Fc 0.4 Nq other than 0.2 Nq since we calculated the SD of background to be the noise level. With higher Fc, it generated slices with a high level noise.

The noise level for six filters was shown in Table 3. Apparently Parzen, Hann and Hamming filters got smoother images. This is reasonable because they are designed to reduce noise effectively. While Shepp–Logan and Butterworth filters, especially the Ramp filter, amplified the high frequencies, which led to a little noisier image.

Total score

Table 4 summarizes the total score for the six filters. Butterworth filter got the highest mean score among all the six filters, because it obtained high contrast and approximate tumour size, and a little low level of noise. At the same time, Butterworth filter obtained the highest maximum value of 93.49 and smallest SD of 12.33. in other words, Butterworth filter enabled to balance the needs of high contrast, low noise, and accurate tumour size.

Figure 8 shows one sample of central slices for the six different filers. As we can see, filters such as Parzen, Hann and Hamming yielded smoother images than the other three filters, they enlarged tumour size and decreased slice

Table 1. Comparison of FWHM for six filters (cm)

Value \ Filter	Parzen	Hann	Hamming	Shepp–Logan	Ramp	Butterworth
Maximum	4.51	4.44	4.29	3.47	3.25	3.22
Minimum	1.85	1.72	1.71	1.63	1.60	1.61
Mean	2.77	2.40	2.30	1.90	1.85	1.83
SD	0.93	0.85	0.77	0.50	0.45	0.39

Table 2. Comparison of contrast for the six filters

Value \ Filter	Parzen	Hann	Hamming	Shepp–Logan	Ramp	Butterworth
Maximum	3.09	3.63	3.69	4.18	4.33	4.32
Minimum	0.58	0.65	0.73	1.27	1.56	1.54
Mean	1.90	2.47	2.58	3.57	3.90	3.86
SD	0.86	1.00	0.97	0.84	0.77	0.75

Table 3. Noise comparison for the six filters

Value \ Filter	Parzen	Hann	Hamming	Shepp–Logan	Ramp	Butterworth
Maximum	0.21	0.21	0.21	0.21	0.26	0.24
Minimum	0.08	0.07	0.08	0.07	0.10	0.08
Mean	0.12	0.11	0.11	0.14	0.17	0.15
SD	0.05	0.04	0.04	0.04	0.05	0.05

Table 4. Summary of total score for the six filters

Value \ Filter	Parzen	Hann	Hamming	Shepp–Logan	Ramp	Butterworth
Maximum	85.13	87 .67	87 .29	91.47	92.55	93.49
Minimum	10.62	9.26	12 .69	32.37	37.72	39.67
Mean	56.12	67 .79	70 .33	78.04	75.71	78.37
SD	27.13	26 .04	23 .58	14.83	14.58	12.33

contrast. Shepp–Logan, Ramp and Butterworth filters yielded similar image quality.

The optimum parameters for Butterworth filter were Fc of 0.45 Nq and Order of 6 (see Figure 9). The Nyquist frequency in this study was 1.28 cycles/cm (0.5 cycles/pixel). So the optimum Fc was 0.58 cycles/cm.

DISCUSSION

Image filtering is one of the most significant factors that greatly influences the quality of clinical SPECT images. It should balance between noise removal and resolution recovery. Currently, a number of filters are available in the 3D reconstruction process. Image quality can be variously affected by filter parameters. Therefore, there is no standard for the type of the filter and the filter parameters in all types of clinical SPECT studies. To choose the optimum filter for an individual case is still a main problem in SPECT image processing.

In this study, Butterworth filter balanced image quality among the six filters. Even though the mean contrast, noise level, and tumour size obtained with the Butterworth filter were not the best, its mean total score was the highest amongst the six filters, which indicated that the Butterworth filter enabled to balance between the needs of high contrast, low noise, and accurate tumour size. This ability is significant for quantification which is greatly dependent on the image quality. The

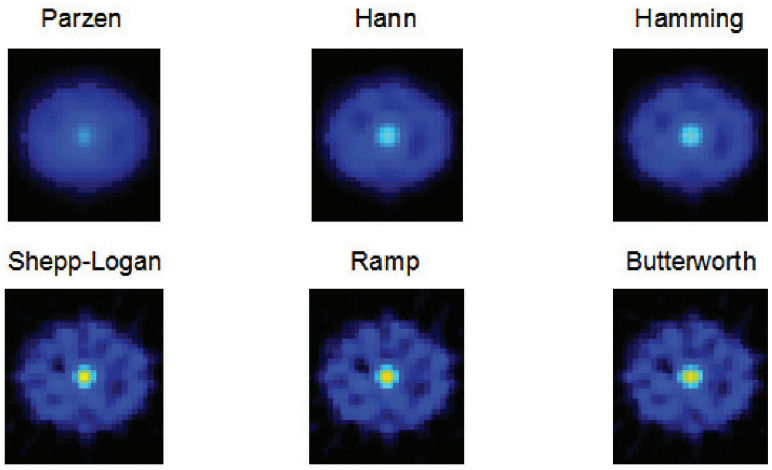

Figure 8. Comparison of central slices obtained from six different filters with cut–off frequency at 0.45 Nq

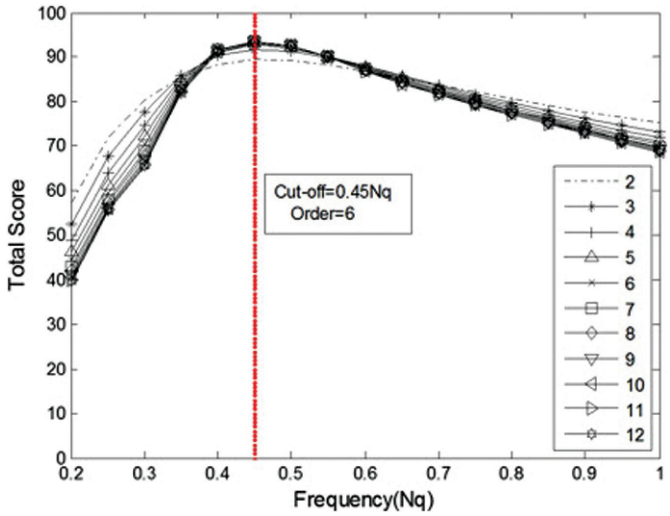

Figure 9. Comparison of Butterworth filter at different cut–off frequencies and order

results showed a good agreement with the previous studies [29, 30], which also showed Butterworth filter to be the best amongst the common used filters for myocardial SPECT imaging. Interestingly, the optimal parameters of Butterworth were well matched with the reported study [29], which indicates that the results of this study may apply to myocardial SPECT imaging.

It is noticeable that the order of Butterworth filter has had little effect on the slice when it was bigger than value of 6. This finding was in agreement with a published study [31], which also found that there was no major difference in their influence on the Fc of 0.5 Nq or above when estimating the optimized values of Butterworth filter for the quantification of the cardiac volumes and left ventricular ejection fraction for technetium–99m gated myocardial SPECT. Therefore, when optimizing the parameters of Butterworth filter, many studies optimized the value of Fc while fixing the value of order [11, 32–34].

CONCLUSION

The selection of an optimal filter during the FBP image reconstruction is vital for cancer detection. The Butterworth filter is suggested to be optimum for breast SPECT imaging owing to its ability to provide a high quality image.

Although an optimum Fc for Butterworth filter in the breast SPECT imaging was found to 0.45 Nq in this study, it actually depends on the image total counts and other properties of the image. Therefore, the optimum Fc need to be decided objectively not subjectively or by "trial and error" method. If parameters of Butterworth were determined subjectively, operator repeatability decreased, so parameters should be set objectively to improve repeatability.

Acknowledgement

The project is funded by the Ministry of Science, Technology and Innovation (UPM) under Science fund Grant No. 5450786 (06-01-04-SF2157) and Natural Science of Chengde Medical University Youth Fund under Grant No. 201727.

List of abbreviation

FBP	Filtered Back Projection
Fc	Cutoff Frequency
FWHM	Full Width at Half Maximum
LEHR	Low-Energy High-Resolution
MBq	MegaBecquere
mCi	MilliCurie
MCNP5	Monte Carlo N-Particle code version 5
NaI	Sodium Iodide
Nq	Nyquist Frequency
PMT	Photomultiplier Tubes
SD	Standard Deviation
SPECT	Single Photon Emission Computed Tomography
99mTc	Technetium-99m
WMC	Wire Mesh Collimator

Conflict of Interests

The authors declare no conflict of interest

Ethical approval

Ethical approval is not required for this study

Consent for publication from the study subjects

Not applicable

REFERENCES

1. Lyra M, Ploussi A. Filtering in SPECT image reconstruction. Int J Biomed Imaging. 2011;2011:1–14.
2. Lyra M, Ploussi A, Rouchota M, Synefia S. Filters in 2D and 3D cardiac SPECT image processing. Cardiol Res Pract. 2014;2014:1–11.
3. Saad WHM, Roslan RE, Mahdi MA, Choong WS, Saion E, Saripan MI. Monte Carlo design of optimal wire mesh collimator for breast tumor imaging process. Nucl Instrum Methods Phys Res Sect A Accel Spectrometers Detect Assoc Equip. 2011;648:254–60.
4. Saripan M, Saad W. Monte Carlo simulation on breast cancer detection using wire mesh collimator gamma camera. IEEE Trans Nucl Sci. 2009;56:1321–4.
5. Roslan RE, Saad WHM, Saripan MI, Hashim S, Choong W–S. The performance of a wire mesh collimator SPECT camera for different breast volumes in prone position. Nucl Instrum Methods Phys Res Sect A Accel Spectrometers Detect Assoc Equip. 2010;619:385–7.
6. Saripan MI, Petrou M, Wells K. Design of a wire–mesh collimator for gamma cameras. IEEE Trans Biomed Eng. 2007;54:1598–612.
7. Wang Y, Tsui BMW, Baird WH, Frey EC, Wessell DE. Investigation of acquisition and image reconstruction parameters for rotating multi–segment slant–hole SPECT. In: Nucl Sci Symp Conf Rec. 2001:2143–6.
8. Baird WH, Frey EC, Tsui BMW, Wang Y, Wessell DE. Evaluation of rotating slant–hole SPECT mammography using Monte Carlo simulation methods. IEEE Trans Nucl Sci. 2003;50(I):105–9.
9. Metzler SD, Bowsher JE, Tornai MP, Pieper BC, Peter J, Jaszczak RJ. SPECT breast imaging combining horizontal and vertical axes of rotation. IEEE Trans Nucl Sci. 2002;49(1):31–6.
10. Perez KL, Cutler SJ. Towards quantification of functional breast images using dedicated SPECT with non–traditional acquisition trajectories. IEEE Trans Nucl Sci. 2011;58:2219–25.
11. Onishi H, Matsutake Y, Matsutomo N, Amijima H. Validation of optimal cut–off frequency using a Butterworth filter in single photon emission computed tomography reconstruction for the target organ? Spatial domain and frequency domain. J Fac Heal Welf. 2010;10:27–36.
12. SIEMENS, SIEMENS SPECT Symbia T: System specifications, [cited 2014 Jul]. Available from: https://3.imimg.com/data3/AC/PC/MY-13438971/gamma-camera.pdf
13. X-5 Monte Carlo Team. MCNP - A general Monte Carlo code n-particle transport code, Version 5. [cited 2014 Jul]. Available from: https://laws.lanl.gov/vhosts/mcnp.lanl.gov/pdf_files/la-ur-03-1987.pdf
14. Bahreyni Toossi MT, Islamian JP, Momennezhad M, Ljungberg M, Naseri SH. SIMIND Monte Carlo simulation of a single photon emission CT. J Med Phys. 2010;35:42–7.
15. Gopal B. Saha, physics and radiobiology of nuclear medicine, 4th ed. New York, NY: Springer; 2013.
16. de Vries DJ, Moore SC, Zimmerman RE, Friedland B, Mueller SP, Lanza RC. Development and validation of a Monte Carlo simulation of photon transport in an anger camera. IEEE Trans Med Imaging. 1990;9:430–8.
17. Cancer Research, Number Stages of Breast Cancer. n.d. [cited 2014 Sept 30]. Available from: http://www.cancerresearchuk.org/aboutcancer/type/breast–cancer/treatment/numberstages–of–breastcancer
18. Sobin LH, Gospodarowicz MK, Wittekind C. TNM Classification of malignant tumours, 7th ed. Chichester,UK: Willey–Blackwell Press; 2009
19. Perez KL. Investigating functional breast image quality and quantification with a dedicated SPECT–CT system. Durham, NC: Duke University; 2011.
20. O'Connor MK, Phillips SW, Hruska CB, Rhodes DJ, Collins DA. Molecular breast imaging: Advances and limitations of a scintimammographic technique in patients with small breast tumors. Clin Imaging. 2007;31:295.
21. Wackers FJ, Berman DS, Maddahi J, Watson DD, Beller GA, Strauss HW, et al. Technetium–99m hexakis 2–methoxyisobutyl isonitrile: Human biodistribution, dosimetry, safety, and preliminary comparison to thallium–201 for myocardial perfusion imaging. J Nucl Med. 1989;30:301–11.
22. Maublant J, de Latour M, Mestas D, Clemenson A, Charrier S, Feillel V, et al. Technetium–99m–sestamibi uptake in breast tumor and associated lymph nodes. J Nucl Med. 1996;37:922–5.
23. Mann SD, Perez KL, McCracken EKE, Shah JP, Wong TZ, Tornai MP. Initial in vivo quantification of Tc–99m Sestamibi uptake as a function of tissue type in healthy breasts using dedicated breast SPECT–CT. J Oncol. 2012;2012:1–7.
24. Gruber GJ, Moses WW, Derenzo SE. Monte Carlo simulation of breast tumor imaging properties with compact, discrete gamma cameras. IEEE Trans Nucl Sci. 1999;46: 2119–2123
25. Dong X. L., Saad WHM, Adnan WAW, Hashim S, Hassan NPM, Nordin AJ, Saripan MI. Simulation of intrinsic resolution of scintillation camera in Monte Carlo environment. In: IEEE Int. Conf. Signal Image Process. Appl., 2013:11–4.
26. Chang L. A method for attenuation correction in radionuclide computed tomography. IEEE Trans Nucl Sci. 1978;25:638–43.
27. IAEA. IAEA quality control atlas for scintillation camera systems [cited 2014 Jul]. Available from: https://www-pub.iaea.org/MTCD/publications/PDF/Pub1141_web.pdf
28. Hruska CB, Connor MKO. Quantification of lesion size, depth, and uptake using a dualhead molecular breast imaging system. Med Phys. 2008;35:1365–77.
29. Takavar A, Shamsipour G, Sohrabi M, Eftekhari M. Determination of optimum filter in myocardial SPECT: A phantom study. Iran J Radiat Res. 2004;1:205–10.
30. Yusoff MNS, Zakaria A. Determination of the optimum filter for qualitative and quantitative 99m Tc myocardial SPECT imaging. Iran J Radiat Res. 2009;6:173–82.
31. Duarte DD, Monteiro MS, Hakmaoui FE, Prior JO, Vieira L, Pires–Jorge JA. Influence of reconstruction parameters during filtered backprojection and ordered–subset expectation maximization in the measurement of the left–ventricular volumes and function during gated SPECT. J Nucl Med Technol. 2012;40:29–36.
32. Minoshima S, Maruno H, Yui N, Togawa T, Kinoshita F, Kubota M, et al. Optimization of Butterworth filter for brain SPECT imaging. Ann Nucl Med. 1993;7:71–7.
33. Sankaran S, Frey EC, Gilland KL, Tsui BMW. Optimum compensation method and filter cutoff frequency in myocardial SPECT: A human observer study. J Nucl Med. 2002;43:432–8.
34. Shibutani T, Onoguchi M, Yamada T, Kamida H, Kunishita K, Hayashi Y, et al. Optimization of the filter parameters in 99mTc myocardial perfusion SPECT studies: The formulation of flowchart. Australas Phys Eng Sci Med. 2016;39:571–81.